

# UC Irvine

## UC Irvine Previously Published Works

### Title

Differential Roles for IL-1 $\alpha$  and IL-1 $\beta$  in *Pseudomonas aeruginosa* Corneal Infection.

### Permalink

<https://escholarship.org/uc/item/18p5t35d>

### Journal

Journal of Immunology, 209(3)

### Authors

Ratitong, Bridget  
Dragan, Morgan  
Anunciado, Charissa  
et al.

### Publication Date

2022-08-01

### DOI

10.4049/jimmunol.2200110

Peer reviewed



Published in final edited form as:

*J Immunol.* 2022 August 01; 209(3): 548–558. doi:10.4049/jimmunol.2200110.

## Differential Roles for IL-1 $\alpha$ and IL-1 $\beta$ in *Pseudomonas aeruginosa* Corneal Infection

Bridget Ratitong<sup>\*,†</sup>, Michaela E. Marshall<sup>‡</sup>, Morgan A. Dragan<sup>†,§</sup>, Charissa M. Anunciado<sup>\*</sup>,  
Serena Abbondante<sup>‡</sup>, Eric Pearlman<sup>\*,†,‡</sup>

<sup>\*</sup>Department of Physiology and Biophysics, University of California, Irvine, Irvine, CA;

<sup>†</sup>Institute for Immunology, University of California, Irvine, Irvine, CA;

<sup>‡</sup>Department of Ophthalmology, University of California, Irvine, Irvine, CA;

<sup>§</sup>Department of Biological Chemistry, University of California, Irvine, Irvine, CA

### Abstract

*Pseudomonas aeruginosa* is an important cause of dermal, pulmonary, and ocular disease. Our studies have focused on *P. aeruginosa* infections of the cornea (keratitis) as a major cause of blinding microbial infections. The infection leads to an influx of innate immune cells, with neutrophils making up to 90% of recruited cells during early stages. We previously reported that the proinflammatory cytokines IL-1 $\alpha$  and IL-1 $\beta$  were elevated during infection. Compared with wild-type (WT), infected *Il1b*<sup>-/-</sup> mice developed more severe corneal disease that is associated with impaired bacterial killing as a result of defective neutrophil recruitment. We also reported that neutrophils are an important source of IL-1 $\alpha$  and IL-1 $\beta$ , which peaked at 24 h postinfection. To examine the role of IL-1 $\alpha$  compared with IL-1 $\beta$  in *P. aeruginosa* keratitis, we inoculated corneas of C57BL/6 (WT), *Il1a*<sup>-/-</sup>, *Il1b*<sup>-/-</sup>, and *Il1a*<sup>-/-</sup>*Il1b*<sup>-/-</sup> (double-knockout) mice with  $5 \times 10^4$  ExoS-expressing *P. aeruginosa*. *Il1b*<sup>-/-</sup> and double-knockout mice have significantly higher bacterial burden that was consistent with delayed neutrophil and monocyte recruitment to the corneas. Surprisingly, *Il1a*<sup>-/-</sup> mice had the opposite phenotype with enhanced bacteria clearance compared with WT mice. Although there were no significant differences in neutrophil recruitment, *Il1a*<sup>-/-</sup> neutrophils displayed a more proinflammatory transcriptomic profile compared to WT with elevations in C1q expression that likely caused the phenotypic differences observed. To our knowledge, our findings identify a novel, non-redundant role for IL-1 $\alpha$  in impairing bacterial clearance.

---

*Pseudomonas aeruginosa* is an opportunistic Gram-negative bacterium that causes serious illnesses following infection of the skin or lungs. It is also a major cause of blinding corneal infections (keratitis) worldwide (1). Intact corneas are typically resistant to infection due to antimicrobial peptides in tear film and tight junctions of epithelial cells that form a physical

---

Address correspondence and reprint requests to Dr. Eric Pearlman, Department of Physiology and Biophysics, University of California, Irvine, 843 Health Sciences Road, Irvine, CA 92697. eric.pearlman@uci.edu.

The online version of this article contains supplemental material.

Disclosures

The authors have no financial conflicts of interest.

barrier (2). However, ocular trauma and poor contact lens hygiene are predisposing factors that facilitate bacterial penetration to the corneal stroma, where they rapidly replicate. *Pseudomonas* keratitis can lead to tissue damage that manifests as severe ocular pain, visual impairment, and can cause permanent blindness if left untreated (3). During the early stages of infection, neutrophils comprise the majority of infiltrating cells in patient corneal ulcers and are associated with elevated gene expression of *Il1a* and *Il1b* (4). Depletion of neutrophils in murine models of microbial keratitis results in significant impairment of bacterial killing, leading to more severe disease (5). We and others have reported that the proinflammatory cytokines IL-1 $\beta$  and IL-1 $\alpha$  are highly elevated in *P. aeruginosa* corneal infections in mice (6, 7). Further, we showed that neutrophils are the main source of IL-1 $\beta$ , and that IL-1 $\beta$ -deficient or IL-1R1-deficient mice have significantly higher bacterial burden (5, 8). However, the role of IL-1 $\alpha$  in *P. aeruginosa* keratitis remains unclear.

IL-1 $\alpha$  is an alarmin and danger-associated molecular pattern that is constitutively expressed by nonhematopoietic cells, such as epithelial cells, to amplify inflammation (9–11). It can also be produced by immune cells in response to stimulation. Recently, we identified neutrophils as an important source of IL-1 $\alpha$  during inflammatory conditions (12). Similar to IL-1 $\beta$ , IL-1 $\alpha$  is first produced as a proform and can be cleaved by calpain into a 17-kDa mature form. Although both IL-1 $\alpha$  and IL-1 $\beta$  signal through IL-1R1, IL-1 $\beta$  bioactivity requires inflammasome activation and cleavage by caspase-1, whereas IL-1 $\alpha$  does not (13, 14). Another key difference between these two cytokines is that pro-IL-1 $\alpha$  contains a nuclear localization sequence in its N-terminal region that allows for nuclear translocation (15). IL-1 $\alpha$  in nonhematopoietic cells localizes to the nucleus during homeostatic conditions and rapidly translocates to the cytosol for release following infection or inflammation (16). However, the role of nuclear IL-1 $\alpha$  in hematopoietic cells is not well understood.

In this study, we examined the role of IL-1 $\alpha$  using a well-defined murine model of *Pseudomonas* keratitis during early-stage infection (5, 8). We demonstrate that IL-1 $\alpha$  peaks at 24 h postinfection (hpi) in infected corneas and is produced by neutrophils and monocytes. In contrast with *Il1b*<sup>-/-</sup> and *Il1a*<sup>-/-</sup>*Il1b*<sup>-/-</sup> double-knockout (DKO) mice, infected corneas of IL-1 $\alpha$ -deficient mice had significantly less bacteria compared with wild-type (WT) mice despite having the same number of neutrophils. RNA sequencing (RNA-seq) of neutrophils isolated from infected corneas revealed a more proinflammatory transcriptomic profile in *Il1a*<sup>-/-</sup> compared with WT neutrophils that likely contributes to the phenotype observed.

## Materials and Methods

### Mice

C57BL/6 mice were purchased from The Jackson Laboratory (Bar Harbor, ME) and bred in-house. All gene knockout (KO) mice are on C57BL/6 background. *Il1a*<sup>-/-</sup>, *Il1b*<sup>-/-</sup>, and *Il1a*<sup>-/-</sup>*Il1b*<sup>-/-</sup> (DKO) mice were originally generated by Dr. Iwakura (University of Tokyo, Japan) as described by Horai et al. (17). *Il1a*<sup>-/-</sup> and DKO mice were graciously provided by Dr. J. Obar (Dartmouth, NH), and *Il1b*<sup>-/-</sup> were obtained from Dr. Gabriel Núñez (University of Michigan). *Pad4*<sup>-/-</sup> were originally provided by Dr. Kerri Mowen at Scripps Research Institute. Mice were bred and housed in the University of California, Irvine (UCI) vivarium.

Age-matched 6- to 8-wk-old male and female mice were used for all experiments. All protocols were approved by UCI Institutional Animal Care and Use Committee.

### Bacterial strains and culture conditions

*P. aeruginosa* ExoS-expressing strains PAO1 and PAO1-GFP were obtained from Dr. A. Rietsch (Case Western Reserve University). Bacteria were grown to midlog phase ( $\sim 1 \times 10^8$  bacteria/ml) in high-salt Luria–Bertoni broth, which enhances expression of the type III secretion system (T3SS) at 37°C with 5% CO<sub>2</sub>, 200 rpm. Bacteria were then washed and resuspended in sterile PBS to  $5 \times 10^4$  bacteria/2  $\mu$ l for all in vivo infections.

### Murine model of *Pseudomonas* keratitis

Corneal epithelial abrasion of 3  $\times$  10 mm was performed using a sterile 30-gauge needle followed by topical infection of  $5 \times 10^4$  PAO1 or PAO1-GFP in 2  $\mu$ l PBS as described previously (5). CFU was quantified at 2 hpi to verify the inoculum for each experiment. At 24, 48, or 72 hpi, mice were euthanized, and corneal opacity and GFP fluorescence were imaged and quantified.

### CFU quantification

At 2 (inoculum), 24, 48, or 72 hpi, whole eyes were collected and homogenized in 1 ml PBS. Serial log dilutions of homogenate were plated on LB plates and incubated at 37°C with 5% CO<sub>2</sub> overnight. Colonies were counted manually, and CFUs were calculated as: (number of colonies  $\times$  dilution factor  $\times$  100 [10  $\mu$ l of the 1 ml was used for plating and dilution]).

### Bone marrow transplantation

Six- to seven-week-old WT or *Illa*<sup>-/-</sup> recipient mice were irradiated at a lethal, single dose of 850 cGy (X-rad 320). Donor bone marrow cells were isolated from hind leg femurs and tibias of WT or *Illa*<sup>-/-</sup> mice. Cells were treated with 1 $\times$  RBC lysis (eBioscience) for 2 min and then washed with sterile PBS. Cells were counted and resuspended at  $1 \times 10^7$  cells/ml PBS. Irradiated recipient mice were anesthetized with isoflurane and transplanted with 100  $\mu$ l ( $1 \times 10^6$  cells) of bone marrow donor cells by retro-orbital injection. Transplanted mice were kept on an antibiotic chow diet (UNI-PRIM) for 3 wk before returning to regular chow for 1–2 wk before infection.

### Cytokine detection

Corneas were dissected and homogenized in 500  $\mu$ l of PBS with Tissue-Lyser II (Qiagen) for 3 min at frequency of 30 hertz. IL-1 $\alpha$ , IL-1 $\beta$ , TNF- $\alpha$ , IL-6, CXCL-2, CXCL-1, CCL2, and IL-1Ra were measured using DuoSet ELISA kits (R&D Systems) according to the manufacturer's protocol. Cytokine concentrations were calculated and plotted as picograms per cornea (pg/cornea).

### Flow cytometry

Dissected corneas were incubated with 3 mg/ml collagenase (C0130; Sigma-Aldrich) in RPMI (Life Technologies), with 1% HEPES (Life Technologies), 1% penicillin-

streptomycin (Life Technologies), and 0.5% BSA (Fisher Bioreagents) for 1 h and 15 min at 37°C. Cells were incubated for 5 min with anti-mouse CD16/32 Ab (BioLegend) to block Fc receptors. Then cells were incubated 20 min at 4°C with anti-mouse CD45-allophycocyanin, Ly6G-BV510, Ly6C-PE-Cy7, CD11b-PETxRed, CCR2-BV421, and F4/80-FITC (BioLegend) and fixable viability dye (BD Biosciences). Cells were washed with FACS buffer and fixed with Cytotfix/Cytoperm (BD Biosciences) for 20 min at 4°C. Fixed cells were washed with PBS.

For intracellular staining, BD Perm/Wash (BD Biosciences) was used to permeabilize cells, and cells were incubated with anti-mouse IL-1 $\alpha$ - PE (BioLegend), citrullinated histone 3 (H3Cit; Abcam), and C1q (courtesy of Dr. F. Lin, Cleveland Clinic) primary Abs at 4°C for 30 min (IL-1 $\alpha$ ) or overnight for unconjugated primary Abs. Cells were washed and resuspended in 100  $\mu$ l Perm/Wash. For unconjugated H3Cit and C1q Abs, cells were incubated with secondary Ab donkey anti-rabbit 647 (Invitrogen) for 1 h at 4°C. Cells were washed with BD Perm/Wash and suspended in 100  $\mu$ l Perm/Wash. An ACEA Novocyte was used for flow cytometric analysis of neutrophils (CD45<sup>+</sup>CD11b<sup>+</sup>Ly6G<sup>+</sup>Ly6C<sup>+</sup>) and monocytes (CD45<sup>+</sup>CD11b<sup>+</sup>Ly6G<sup>-</sup>Ly6C<sup>hi</sup>CCR2<sup>+</sup>). NovoExpress software was used for data analysis, calculation of mean fluorescent intensity (MFI), cell frequency, and cell count. Amnis ImageStream was used for imaging flow cytometry, and analysis was performed on Amnis IDEAS software.

## Histology

At 24 or 48 hpi, the back of eyes was punctured with a 23-gauge needle and placed in 4% PFA for at least 48 h. Eyes were then paraffin embedded and 8- $\mu$ m sections were examined by H&E staining. In brief, slides were stained with hematoxylin (Sigma-Aldrich) and rinsed in running water before dipping in bluing reagent (Fisher Scientific) and counterstaining with eosin (Sigma-Aldrich). Slides were then dehydrated in ethanol followed by xylene. Slides were then mounted using Permount (Fisher Scientific) and imaged.

## Immunofluorescence staining of whole corneas

At 24 hpi, whole eyes were embedded in OCT (Sakura) and frozen in dry ice. Blocks were sectioned at 8  $\mu$ m for subsequent immunofluorescence staining. In brief, slides were thawed and placed in 100% acetone at -20°C for 10 min. Sections were then fixed with 4% PFA (Thermo Scientific), washed in PBS (Life Technologies), and incubated 1 h with Fc block (BioLegend) and normal donkey serum (Jackson ImmunoResearch) diluted in 1% BSA (Fisher Bioreagents). Primary Abs Ly-6G/Ly-6C mAb NIMP-R14 (Invitrogen) and Rabbit anti-H3Cit (Abcam) were diluted 1:50 and 1:100, respectively, in blocking buffer and incubated overnight at 4°C. Slides were washed three times for 10 min with PBS. Secondary Abs goat anti-Rat 647 (Invitrogen) and goat anti-Rabbit 488 (Invitrogen) were diluted 1:1000 and 1:500, respectively, in blocking buffer and added to sections for 1 h at room temperature. Slides were then washed four times for 10 min in PBS and counterstained with DAPI. Finally, slides were mounted using Vectashield Antifade Mounting Medium (Vector Laboratories), and sections were imaged on a Keyence All-in-One Fluorescence Imager, BZ-X series (Keyence). Image contrast and brightness were adjusted to the same setting on all images.

## RNA-seq and analysis

Corneas were digested as previously described and pooled (4 pooled corneas = 1 n). Live CD45<sup>+</sup>Ly6G<sup>+</sup>Ly6C<sup>+</sup> corneal neutrophils were FACS isolated with BD FACSAria II sorter (UCI flow cytometry core). RNA was isolated from sorted samples with RNeasy Micro kit (Qiagen) and submitted to UCI Genomics core for quality control, library building, and sequencing. In brief, RNA was quantified using the NanoDrop ND-1000 spectrophotometer (Thermo Fisher) and quality checked using the Agilent Bioanalyzer 2100 (Agilent). Library construction was performed according to the Clontech SMART-Seq v4 Ultra Low Input RNA/Nextera XT Library Preparation Guide. mRNA was enriched from 1 µg total RNA using oligo dT magnetic beads. The enriched mRNA was chemically fragmented for 3 min, followed by reverse transcription to generate cDNA. The resulting cDNA was cleaned using AMPure XP beads and end repaired, and the 3' ends were adenylated. Illumina barcoded adapters were ligated on the ends, and the adapter-ligated fragments were enriched by nine cycles of PCR. The resulting libraries were validated by qPCR and sized by Agilent Bioanalyzer DNA high-sensitivity chip. The barcoded cDNA libraries were multiplexed on the NovaSeq 6000 platform to yield 100-bp paired-end reads. FASTQ files were trimmed using Trimmomatic version 0.39, aligned to the mm10 genome, and counted using STAR version 2.7.8a. Differential expression analysis was performed using DESeq2 version 1.24.0 on R version 3.6.0.

## Western blot

At 24 hpi, corneas were dissected and homogenized in 1× cell lysis buffer (Cell Signaling) containing 5 mM di-isopropyl fluorophosphates (Sigma-Aldrich) to inactivate neutrophil proteases. Lysates were cleared by centrifugation at 10,000 × *g* for 10 min. Protein concentration was calculated using a BCA protein assay kit (Thermo Fisher). A total of 50 µg protein from lysates, 1× SDS (from 5 × stock), and ultrapure water (Invitrogen) was mixed and boiled for 10 min at 95°C on a heating block. Samples were loaded into 4–20% mini-PROTEAN, 10-well, 50-µl TGX precast protein gels (Bio-Rad). Proteins were transferred to a nitrocellulose membrane using a Bio-Rad Transblot Turbo transfer system. Membranes were blocked with 5% milk in TBST for 1 h at room temperature. Primary Abs rabbit anti-C1q clone 1151 (Dr. Tenner, UCI), mouse anti-β-actin (Santa Cruz Biotechnology), hamster anti-IL-1α (eBioscience), rabbit anti-Lamin B1 (Abcam), mouse anti-IL-1R2 (Santa Cruz Biotechnology), and rabbit anti-GAPDH (BioLegend) were diluted in 5% milk and gently rocked overnight at 4°C. Membranes were washed with 1× TBST buffer three times for 10 min. HRP-conjugated secondary Abs against rabbit (Cell Signaling), mouse (Cell Signaling), or hamster (Santa Cruz Biotechnology) were diluted in 5% milk and incubated at room temperature for 1 h. West Femto Maximum SuperSignal (Thermo Fisher) was used to enhance the signal before the membrane was imaged with ChemiDoc MP Imaging System (Bio-Rad). Band intensity was quantified using Image Lab software.

## In vitro neutrophil functional analysis

Casein (9%; Sigma-Aldrich) was injected i.p. 16 and 3 h before peritoneal lavage to induce sterile inflammation. Cells were recovered from the inflamed peritoneal cavity after lavage

with 10 ml cold sterile PBS. Negative selection (STEMCELL Technologies) beads were used to enrich for neutrophils according to the manufacturer's guidelines and generated >97% neutrophils. Neutrophils were plated at  $2 \times 10^6$  cells/ml RPMI (Life Technologies) for functional analysis.

**Neutrophil extracellular trap formation.**—Neutrophils were preincubated with SYTOX (Invitrogen) for 30 min at 37°C before addition of 25 ng PMA (Sigma) or PAO1 at a multiplicity of infection (MOI) of 30. Fluorescent signal was read over 16 h using a Cytation5 imaging plate reader (Agilent). The area under the curve (AUC) was calculated from the average of the curves of technical replicates.

**Reactive oxygen species.**—Neutrophils were preincubated with luminol (Sigma) for 30 min before stimulation. A total of 25 ng PMA (Sigma) or PAO1 at MOI of 30 was added and immediately read on the Cytation5 for 90 min. AUC was calculated from the average of the curves of technical replicates.

**In vitro neutrophil bacterial killing.**—A total of  $2 \times 10^5$  cells were plated per well in a 96-well plate (CytoOne). PAO1 was added at MOI of 30 in duplicates except for the negative control wells and incubated at 37°C with 5% CO<sub>2</sub>. After 15 min, 400 µg/ml gentamicin (Sigma) was added to kill extracellular bacteria. After an additional 30-min incubation with gentamicin, cells were centrifuged at  $300 \times g$  for 5 min and washed twice with PBS. 0.1% Triton-X (Fisher Scientific) in PBS was used to lyse the cells, and bacteria were serially diluted and plated on LB plates. CFU was counted after an overnight incubation at 37°C, 5% CO<sub>2</sub>.

### Statistical analysis

Statistical analysis was determined by unpaired *t* tests, ordinary one-way ANOVA with Dunnett's multiple comparisons test, Brown–Forsythe and Welch ANOVA with Dunnett's T3 multiple comparisons test, or two-way ANOVA with Tukey's multiple comparisons test (detailed in the figure legends) using GraphPad Prism software. Outliers were removed with robust regression and outlier removal method ( $Q = 1\%$ ) using GraphPad Prism software. Error bars indicate mean  $\pm$  SEM, and  $p < 0.05$  is considered significant. The number of biological replicates for each experiment can be found in the figure legends. Asterisks denote *p* values as follows in each figure: <sup>ns</sup>*p* = not significant, \**p* < 0.05, \*\**p* < 0.01, \*\*\**p* < 0.001, \*\*\*\**p* < 0.0001.

## Results

### Neutrophils and monocytes are the major sources of IL-1 $\alpha$ during *P. aeruginosa* keratitis

We first measured IL-1 $\alpha$  and IL-1 $\beta$  concentrations in the corneas of C57BL/6 (WT) mice after infection with  $5 \times 10^4$  *P. aeruginosa* (PAO1 strain) by ELISA. Consistent with previous reports, IL-1 $\alpha$  and IL-1 $\beta$  levels peaked at 24 hpi, coinciding with infiltration of neutrophils and monocytes (Fig. 1A, 1B). IL-1 $\alpha$  and IL-1 $\beta$  were undetectable in PBS mock-infected corneas (data not shown).

Previous studies identified neutrophils as the primary source of IL-1 $\beta$  in bacteria-infected corneas (5). To identify the cellular source of IL-1 $\alpha$ , we examined intracellular IL-1 $\alpha$  in infiltrating myeloid cells at 24 hpi by flow cytometry. Cells were gated on live, single CD45<sup>+</sup> CD11b<sup>+</sup> cells, and neutrophils were defined by Ly6G<sup>+</sup>Ly6C<sup>+</sup> events, while monocytes were Ly6G<sup>-</sup>Ly6C<sup>+</sup> and CCR2<sup>+</sup> (Fig. 1C, gating strategy in Supplemental Fig. 2B). Consistent with previous studies from our laboratory (5), we found that 80–90% of CD45<sup>+</sup> infiltrating cells at early-stage infection were neutrophils and <10% were monocytes. Intracellular cytokine staining revealed that IL-1 $\alpha$  was produced by neutrophils and monocytes recruited to infected corneas (Fig. 1D). *Il1a*<sup>-/-</sup> cells were used as fluorescence minus one control. MFI levels were significantly higher than the control, indicating that both cell types are major sources of IL-1 $\alpha$ . IL-1 $\alpha$ -PE MFI levels were higher in monocytes than in neutrophils, indicative of higher production on a per-cell basis. However, neutrophils greatly outnumber monocytes in infected corneas and, therefore, are a major source of IL-1 $\alpha$  in the cornea.

Although corneal epithelial cells release IL-1 $\alpha$  during necrotic cell death (11), we found that IL-1 $\alpha$  and IL-1 $\beta$  were undetectable at 4 hpi and in PBS mock infection, suggesting that infiltrating myeloid cells rather than resident corneal cells are the primary source of IL-1 $\alpha$  during infection. In support of this, Western blot analysis of whole cornea homogenates from mock-infected corneas at 24 hpi revealed no detectable IL-1 $\alpha$  compared with PAO1-infected corneas (Supplemental Fig. 1A). Further, there was no significant increase in IL-1 $\alpha$  release by human corneal epithelial cells in response to incubation with LPS or PAO1. Taken together, we conclude that epithelial cells are not an important source of IL-1 $\alpha$  or IL-1 $\beta$  during *P. aeruginosa* keratitis (Supplemental Fig. 1B, 1C).

### Differential roles for IL-1 $\alpha$ and IL-1 $\beta$ in *P. aeruginosa* keratitis

Previous studies from our laboratory showed impaired bacterial clearance in *Il1b*<sup>-/-</sup> mice that was associated with impaired recruitment of neutrophils to infected corneas (5). To determine whether there is a role for IL-1 $\alpha$  during *P. aeruginosa* keratitis, we infected WT, *Il1a*<sup>-/-</sup>, *Il1b*<sup>-/-</sup>, and DKO mice with  $5 \times 10^4$  PAO1-GFP and examined corneal opacity, GFP fluorescence, and bacterial burden. At 24 hpi, there were no significant differences in corneal opacity among the four genotypes despite GFP levels seemingly higher in the *Il1b*<sup>-/-</sup> and DKO mice and lower in *Il1a*<sup>-/-</sup> compared with WT mice. However, by 48 hpi, *Il1b*<sup>-/-</sup> and DKO mice had noticeably higher corneal opacity compared with WT (Fig. 2A, 2B). Surprisingly, *Il1a*<sup>-/-</sup> mice had the opposite phenotype with significantly lower corneal opacity at 48 hpi compared with WT, suggesting that IL-1 $\alpha$  plays a distinct role from IL-1 $\beta$  by contributing to disease exacerbation. Although not statistically significant, the DKO mice had slightly more disease and bacterial burden than *Il1b*<sup>-/-</sup> mice. However, when both IL-1 $\alpha$  and IL-1 $\beta$  are absent, the *Il1b*<sup>-/-</sup> phenotype appears to be dominant, indicating that there are redundant and nonredundant roles for IL-1 $\alpha$  and IL-1 $\beta$ .

Consistent with corneal opacity and GFP levels, bacterial burden was higher in *Il1b*<sup>-/-</sup> and DKO compared with WT corneas at both 24 and 48 hpi. In marked contrast, there was a log-fold lower CFU in *Il1a*<sup>-/-</sup> compared with WT mice at 48 and 72 hpi (Fig. 2C, 2D).

Because *Il1b*<sup>-/-</sup> and DKO mice were at risk for corneal perforation at 48 hpi, we did not extend the experiment to 72 hpi for these genotypes.

Next, to determine whether it is IL-1 $\alpha$  deficiency in infiltrating immune cells or resident cells in the cornea that are causing enhanced bacterial killing, we performed bone marrow transplant experiments. WT or *Il1a*<sup>-/-</sup> donor bone marrow cells were i.v. injected into irradiated WT (WT-WT, KO-WT) or *Il1a*<sup>-/-</sup> (WT-KO, KO-KO) recipient mice. After 5 wk, mice were infected with  $5 \times 10^4$  PAO1, and CFU was quantified at 48 hpi. We found no differences between the WT-WT and the WT-KO group compared with non-transplanted WT mice, but we did find significantly lower CFUs in the KO-WT and KO-KO groups, indicating that IL-1 $\alpha$  deficiency in immune cells and not resident cells mediate enhanced bacterial clearance (Fig. 2E). Collectively, these findings demonstrate that IL-1 $\alpha$ , in contrast with IL-1 $\beta$ , impairs rather than enhances bacterial killing.

### Myeloid cell recruitment is delayed in infected *Il1b*<sup>-/-</sup> but not *Il1a*<sup>-/-</sup> corneas

Previous studies from our laboratory and others reported that neutrophils are critical for bacterial clearance in infected corneas (5, 18, 19). To address whether the differences observed in bacterial burden between WT, *Il1a*<sup>-/-</sup>, *Il1b*<sup>-/-</sup>, and DKO mice are due to changes in cellular infiltration, we examined *P. aeruginosa*-infected eyes by histology and by flow cytometry at 24 and 48 hpi. Histological examination of corneal sections revealed pronounced cellular infiltration in WT and *Il1a*<sup>-/-</sup> central corneas at 24 hpi compared with healthy corneas (Fig. 3A, Supplemental Fig. 2A). In contrast, cellular infiltration was detected in the periphery, but not the central corneas of *Il1b*<sup>-/-</sup> and DKO corneas, reflecting the ring-like pattern of corneal opacity shown in Fig. 2A. By 48 hpi, *Il1b*<sup>-/-</sup> and DKO corneas exhibited a marked increase in recruited cells compared with WT and *Il1a*<sup>-/-</sup> corneas.

Infiltrating cells were identified and quantified by flow cytometry as total CD45<sup>+</sup>CD11b<sup>+</sup> cells, Ly6G<sup>+</sup> neutrophils, and Ly6G<sup>-</sup>Ly6C<sup>+</sup>CCR2<sup>+</sup> monocytes (gating strategy shown in Supplemental Fig. 2B). Consistent with the histology, we found significantly fewer neutrophils and monocytes in *Il1b*<sup>-/-</sup> and DKO mice at 24 hpi (Fig. 3B, 3C). Although *Il1a*<sup>-/-</sup> corneas showed no significant differences in total CD45<sup>+</sup>CD11b<sup>+</sup> and neutrophil cell counts compared with WT, there were significantly fewer monocytes at 24 hpi (Fig. 3B, 3C).

### Cytokine production in infected corneas

To address whether the lower monocyte number in *Il1a*<sup>-/-</sup> compared with WT mice is due to differences in cytokine production, we quantified cytokines and chemokines in infected corneas by ELISA. For IL-1 family members, we found no differences in IL-1 $\beta$  production between infected WT and *Il1a*<sup>-/-</sup> corneas (Fig. 4A). However, *Il1b*<sup>-/-</sup> corneas had less IL-1 $\alpha$ , which correlates with the lower numbers of neutrophils and monocytes in the cornea at 24 hpi (Fig. 4B). There were no significant differences in IL-1Ra (Fig. 4C). For chemokines, CXCL2 production was elevated in *Il1b*<sup>-/-</sup> and DKO compared with *Il1a*<sup>-/-</sup> and WT corneas (Fig. 4D), which reflects the delayed recruitment of neutrophils migrating into central cornea (Fig. 3A, 3C). There were no differences in CXCL1 or CCL2 among the groups (Fig. 4E, 4F). Lastly, *Il1b*<sup>-/-</sup> had significantly higher levels of TNF- $\alpha$  compared with

WT (Fig. 4G); however, the low concentration of TNF- $\alpha$  per cornea suggests that it is not physiologically relevant. We also found significantly less IL-6 in *Il1a*<sup>-/-</sup> and DKO corneas compared with WT that was not apparent in *Il1b*<sup>-/-</sup>, indicating that IL-6 secretion is partially IL-1 $\alpha$  dependent and IL-1 $\beta$  independent (Fig. 4H). IFN- $\beta$ , IFN- $\gamma$ , IL-10, and GM-CSF were below the threshold of detection (data not shown).

As IL-6 levels in all groups were <100 pg/ml, the major conclusion from these data is that differences in cytokine production do not appear to explain the lower monocyte numbers or the clinical phenotype of *Il1a*<sup>-/-</sup> mice. However, the increased CXCL2 production in *Il1b*<sup>-/-</sup> and DKO mice at 24 hpi may account for the increased recruitment of neutrophils in infected corneas at 48 hpi.

### IL-1 $\alpha$ deficiency does not affect neutrophil effector functions

Although there were no differences in neutrophil recruitment to the corneas between WT and *Il1a*<sup>-/-</sup> mice, we examined whether there were functional differences. To analyze neutrophil extracellular trap formation (NETosis) in infected corneas, we used frozen sections of infected WT and *Il1a*<sup>-/-</sup> corneas for immunofluorescence of H3Cit and the neutrophil marker NIMP-R14. We found no defects in histone citrullination in *Il1a*<sup>-/-</sup> compared with WT corneas in vivo (Fig. 5A). In addition, we quantified intracellular H3Cit<sup>+</sup> neutrophils ex vivo from infected corneas by flow cytometry using infected *Pad4*<sup>-/-</sup> corneas as a negative control and found no significant difference between WT and *Il1a*<sup>-/-</sup> (Fig. 5B, 5C, Supplemental Fig. 3A).

In vitro, neutrophils were isolated from the peritoneal cavity after inducing sterile inflammation, and cells were enriched by negative bead selection and stimulated with PMA or PAO1 at MOI 30 to examine NETosis, reactive oxygen species (ROS), and bacterial killing. NETs were quantified by SYTOX Green, which binds to extracellular DNA and is quantified by fluorescence. Although extracellular DNA was elevated in PMA- and PAO1-stimulated neutrophils compared with unstimulated media control, we found no significant differences between WT and *Il1a*<sup>-/-</sup> neutrophils under any conditions (Fig. 5D, time-course graphs in Supplemental Fig. 3B).

To determine whether there is a difference in ROS production, we incubated peritoneal neutrophils from WT and *Il1a*<sup>-/-</sup> mice for 90 min with PMA or PAO1 in the presence of luminol. PMA was used as a positive control for ROS production because PAO1 is known to inhibit ROS (20). Again, no differences were observed between WT and *Il1a*<sup>-/-</sup> neutrophils with either stimulus (Fig. 5E, time course shown in Supplemental Fig. 3C).

Further, we assessed whether there is a difference between WT and *Il1a*<sup>-/-</sup> neutrophils in bacterial killing in vitro (20). Neutrophils were incubated with PAO1 for 15 min, and extracellular bacteria were killed with gentamicin. Antibiotics were removed, and neutrophils were lysed in a mild detergent to quantify the CFUs of phagocytosed bacteria. We observed no differences in CFUs between WT and *Il1a*<sup>-/-</sup> in vitro (Fig. 5F). Taken together, results from these studies indicate that these neutrophil effector activities are not affected by the absence of IL-1 $\alpha$ .

### Nuclear localization of IL-1 $\alpha$ occurs in dendritic cells, but not neutrophils

IL-1 $\alpha$  and IL-1 $\beta$  play distinct roles in bacterial clearance from infected corneas (Fig. 2) despite both signaling through IL-1R1. One major difference between the two cytokines is that full-length IL-1 $\alpha$  contains a highly conserved nuclear localization sequence, whereas IL-1 $\beta$  does not (21). Nuclear translocation of IL-1 $\alpha$  has been reported in macrophages and microglia without a clear function (22, 23). Therefore, we next addressed whether IL-1 $\alpha$  localizes to the nucleus in neutrophils. Bone marrow–derived dendritic cells (BMDCs) were used as a positive control because they produce high levels of IL-1 $\alpha$  in response to stimuli such as LPS (12, 14). IL-1 $\alpha$  localization was first examined by ImageStream imaging flow cytometry, where we found nuclear localization of IL-1 $\alpha$  in ~35% of BMDCs stimulated with LPS (Fig. 5G, quantification shown in Supplemental Fig. 3D). As a second approach, nuclear and cytoplasmic extracts from stimulated BMDCs were analyzed by Western blot, confirming the presence of IL-1 $\alpha$  in the nucleus (Fig. 5H). In contrast, we found that IL-1 $\alpha$  is localized in the cytoplasm, but not the nucleus, of in vitro–stimulated neutrophils and ex vivo neutrophils isolated from infected corneas (Fig. 5I, 5J, Supplemental Fig. 3D). These findings indicate that the distinct roles for IL-1 $\alpha$  and IL-1 $\beta$  in bacterial keratitis are not a consequence of IL-1 $\alpha$  nuclear localization in neutrophils.

### Neutrophils from infected *Il1a*<sup>-/-</sup> corneas have a more proinflammatory transcriptomic profile compared with WT neutrophils

Although there was no difference in neutrophil recruitment to infected WT and *Il1a*<sup>-/-</sup> corneas and no differences in in vitro functional analyses, we sought to determine whether there are gene expression differences between WT and *Il1a*<sup>-/-</sup> neutrophils in vivo by RNA-seq. WT and *Il1a*<sup>-/-</sup> mice were infected with  $5 \times 10^4$  PAO1 and at 24 hpi, live Ly6G<sup>+</sup>Ly6C<sup>+</sup> neutrophils were sorted from the corneas for bulk RNA-seq. Four infected corneas were pooled for each sample. From our sequencing data, we observed differences in gene expression between neutrophils from infected WT and *Il1a*<sup>-/-</sup> corneas. Most notably, inflammatory genes, including *C1qb*, *Msr1*, *Tnfrsf9*, and *Pf4*, were upregulated in *Il1a*<sup>-/-</sup> neutrophils (Fig. 6A, 6B). To identify differences in biological processes and pathways, we annotated differentially expressed genes using Metascape analysis (24). Gene Ontology terms for “Regulation of leukocyte activation,” “Regulation of adaptive immune response,” and “Cytokine activity” were enriched in the *Il1a*<sup>-/-</sup> neutrophils compared with WT (Fig. 6C).

*C1qb* is one of the genes of interest that are upregulated in *Il1a*<sup>-/-</sup>. C1qb, along with C1qa and C1qc, chains form the C1q molecule that regulates phagocytosis and cytokine production (25). C1q is part of the classical complement pathway initiation complex that cleaves C4 and C2 to generate C4b2b, which leads to cleavage of C3 and C5 (25). We therefore analyzed our RNA-seq data for expression of additional complement genes. We found that *C3*, *Hc* (C5), and *C5ar1* gene expression levels were high in neutrophils; however, *C1qb* was the only complement gene that was elevated in neutrophils from infected *Il1a*<sup>-/-</sup> corneas (Fig. 6D).

To verify that C1q was elevated in *Il1a*<sup>-/-</sup> neutrophils, we dissected and homogenized infected corneas at 24 hpi for detection of C1q protein by Western blot (WT and

C1q<sup>-/-</sup> plasma were used as controls). Although C1q was detectable in WT mouse corneas, quantification of C1q over  $\beta$ -actin bands (loading control) showed that there was significantly more C1q protein in *Il1a*<sup>-/-</sup> corneas (Fig. 6E). Further, immunofluorescence staining of C1q in infected corneas showed higher levels in *Il1a*<sup>-/-</sup> compared with WT and *Il1b*<sup>-/-</sup> in the central cornea (Supplemental Fig. 4A–C). Neutrophil-specific production of C1q in infected corneas was also quantified by flow cytometry. Although C1q<sup>+</sup> neutrophils were <3%, we found higher frequency of C1q<sup>+</sup> neutrophils in infected *Il1a*<sup>-/-</sup> compared with WT corneas (Supplemental Fig. 4D, 4E). Overall, these data show that infected corneas of IL-1 $\alpha$ -deficient mice have a more proinflammatory transcriptomic profile, including elevated C1q, which may contribute to enhanced bacterial clearance.

## Discussion

IL-1 $\alpha$  and IL-1 $\beta$  are proinflammatory cytokines that are highly upregulated during infection or sterile inflammation. We and others have identified IL-1 $\beta$  as a critical regulator of immune cell recruitment and subsequently bacterial clearance in a well-defined model of *P. aeruginosa* keratitis (5, 26). In addition, we reported that neutrophils comprise >80% of infiltrating cells during early-stage infection and are the main source of IL-1 $\beta$  in bacterial and fungal keratitis (5, 27). Recently, we reported that neutrophils are also an important source of IL-1 $\alpha$  with an exosome-mediated secretion mechanism that is distinct from Gasdermin D-mediated IL-1 $\alpha$  secretion by dendritic cells and macrophages (12). We further demonstrate in this study that neutrophils and monocytes are the main source of IL-1 $\alpha$  in vivo during *P. aeruginosa* keratitis, and that IL-1 $\alpha$  and IL-1 $\beta$  have nonredundant roles in cellular recruitment and bacterial killing in the cornea.

*P. aeruginosa* is a Gram-negative bacterium that expresses a T3SS used to inject T3SS effector proteins into host cells (28). The effector protein ExoS inhibits ROS production by neutrophils and disrupts actin cytoskeleton to prevent phagocytosis (20, 29). *P. aeruginosa* strains expressing both ExoS and ExoU are rare, and the majority of clinical isolates are ExoS-expressing strains (4). Distinct from other effector proteins, ExoU is a highly cytotoxic phospholipase that causes rapid cell death akin to necrosis (28, 30). ExoU-expressing strains are more virulent than the ExoS-expressing strain PAO1 used in this study (8).

It is important to note that there are differences in responses to ExoS- or ExoU-expressing strains. We reported that neither IL-1 $\alpha$  nor IL-1 $\beta$  was sufficient to provide protection during corneal infection with an ExoU-expressing *P. aeruginosa* strain, 19660, while *Il1r1*<sup>-/-</sup> and *Il1a*<sup>-/-</sup>*Il1b*<sup>-/-</sup> (DKO) had impaired bacterial clearance and more severe disease (8). These observations indicate that during infection with an ExoU-expressing strain, IL-1 $\alpha$  and IL-1 $\beta$  play redundant roles. Conversely, IL-1 $\beta$  was sufficient for protection in an infection with the ExoS-expressing PAO1 (5), which we replicated in this study. We now find that IL-1 $\alpha$  has a distinct role from IL-1 $\beta$  by exacerbating disease and impairing bacterial killing. Because *Il1b*<sup>-/-</sup> mice display delayed cellular recruitment and impaired bacterial clearance that is mirrored in the DKO mice, we conclude that the *Il1b*<sup>-/-</sup> phenotype is dominant in this model. Together, these studies indicate that there is a differential requirement of IL-1 $\alpha$  and IL-1 $\beta$  for protection against ExoS compared with ExoU-expressing strains of *P. aeruginosa*.

Further, in a lung infection model with a different ExoU-expressing *P. aeruginosa* strain, PA103, neutrophil recruitment was IL-1 $\alpha$  dependent and IL-1 $\beta$  independent. This finding was based on ExoU activity because infection with ExoU PA103 displayed the opposite phenotype, where IL-1 $\beta$ , instead of IL-1 $\alpha$ , is required for neutrophil recruitment to the lungs (31), further illustrating that IL-1 $\alpha$  and IL-1 $\beta$  can play distinct roles in response to T3SS effectors produced by *P. aeruginosa*.

A selective role for IL-1 $\alpha$  was also reported during infections with *Legionella pneumophila*, *Streptococcus pneumoniae*, and *Aspergillus fumigatus*. In an in vivo murine model of *Legionella pneumophila* infection, only IL-1 $\alpha$ , but not IL-1 $\beta$ , is essential for neutrophil recruitment to the lungs (32). Further, IL-1 $\alpha$  and IL-1 $\beta$  were shown to have nonredundant roles during *S. pneumoniae* infection that is based on spatial restriction in vivo (33). Pulmonary infection with a virulent strain of *Aspergillus fumigatus* also showed that IL-1 $\alpha$ , rather than IL-1 $\beta$ , is critical for neutrophil recruitment and was required for survival of infected animals (34, 35). However, IL-1 $\alpha$  is not necessary in *A. fumigatus* corneal infection (data not shown), while IL-1 $\beta$  is important for this model (27). Taken together, these findings indicate that the relative contributions of IL-1 $\alpha$  and IL-1 $\beta$  to disease severity and microbial killing are dependent on the sites of infection and the infectious agents.

The conflicting effects of IL-1 $\alpha$  and IL-1 $\beta$  on bacterial burden during corneal infection with PAO1 point to differing roles played by these cytokines despite binding to the same receptor. Because IL-1 $\alpha$  was found only in the cytoplasm, there is no evidence of a nuclear role for IL-1 $\alpha$  in neutrophils. We also found that there were no intrinsic differences in neutrophil ROS production, NETosis, or bacterial killing between WT and *Il1a*<sup>-/-</sup> in vitro, suggesting an indirect, but selective, role for IL-1 $\alpha$  signaling. Because IL-1 $\alpha$  and IL-1 $\beta$  share similar protein structures and signal through the same receptor, IL-1R1, their roles were often considered redundant (36). However, accumulating evidence now suggest they each play distinct roles during different pathological conditions (37). For instance, in a dextran sulfate sodium-induced model of intestinal inflammation, IL-1 $\alpha$  plays a key role in driving inflammation, while IL-1 $\beta$  promotes repair and reconstitution of the epithelial barrier (38). Similarly, in the tumor microenvironment, IL-1 $\alpha$  stimulates antitumor cell immunity, whereas IL-1 $\beta$  produced by myeloid-derived suppressor cells (MDSCs) induces immunosuppression (39, 40). Moreover, IL-1 $\alpha$  is the predominant IL-1R1 determinant of mortality in a neonatal sepsis model, while IL-1 $\beta$  was detected but unnecessary for lethality (41). Our current study adds to the accumulating evidence supporting the paradoxical, nonredundant roles of IL-1 $\alpha$  and IL-1 $\beta$ .

One possible mechanism for the differential roles of IL-1 $\alpha$  and IL-1 $\beta$  observed in vivo could be the spatial and temporal expression of IL-1R1 and IL-1R2. A recent study suggested the bioavailability of IL-1 $\alpha$  and IL-1 $\beta$  in different tissues as a possible mechanism for their nonredundant roles (33). Although we found no differences in IL-1 $\beta$  levels in *Il1a*<sup>-/-</sup> corneas, we examined expression of IL-1R2, the IL-1 decoy receptor, and found it highly expressed in the corneas of both WT and *Il1a*<sup>-/-</sup> mice (Supplemental Fig. 4F, 4G). IL-1R2 has a higher affinity for IL-1 $\beta$  at 10<sup>-10</sup> M, which is 100 times higher than its affinity for IL-1 $\alpha$  (42, 43). Because we found high levels of IL-1R2 in the corneas, it is likely that IL-1 $\beta$  signaling is dampened by the decoy receptor in WT animals, allowing IL-1 $\alpha$  signaling to be

dominant. In *Il1a*<sup>-/-</sup>, signaling is solely induced by IL-1 $\beta$ , which has a protective role in *P. aeruginosa* keratitis. However, the bioavailability of IL-1 $\alpha$  versus IL-1 $\beta$  to signal IL-1R1 in vivo requires further investigation.

In this study, we examined the transcriptomic profile of neutrophils from WT and IL-1 $\alpha$ -deficient corneas to identify genes that are selectively expressed in the absence of IL-1 $\alpha$ . C1qb was one of the genes that is upregulated in *Il1a*<sup>-/-</sup> neutrophils. Complement proteins are present at low levels in healthy corneas; however, serum complement and complement components secreted by infiltrating cells lead to activation of the complement cascade that contributes to disease pathology during infection or inflammatory conditions (44). C1q is part of the classical complement pathway initiator that cleaves C4 and C2, resulting in activated C3 convertase (25). Cleaved C3 components lead to (1) activation of the membrane attack complex (C5b-9) and (2) exert direct effector function to directly kill bacteria (45). Although we did not find differences in neutrophil C3 expression in the corneas, it is likely that the increased production of C1q would lead to more C3 cleavage and facilitate bacterial killing. In addition, novel roles of C1q that are independent from the classical complement pathway have been described; this includes Ab-independent activation of C1 by direct binding to bacteria and enhancing Fc $\gamma$ R-mediated phagocytosis (46). Future studies will examine these functions of C1q in the cornea and determine whether they have a role in bacterial killing.

In summary, this study revealed an unexpected role for IL-1 $\alpha$  during *Pseudomonas* keratitis that is distinct from IL-1 $\beta$ , and identified monocytes and neutrophils as the primary sources of IL-1 $\alpha$ . Our observations raise several questions that will require further studies, including identifying differences in IL-1 signaling, the relative concentration of bioactive forms of IL-1 $\alpha$  and IL-1 $\beta$  under different infectious and inflammatory conditions, and signal outcome in different IL-1R1-expressing cells (37). It is also unclear how IL-1 $\alpha$  deficiency contributes to upregulation of C1q and if it is due to IL-1 $\beta$  signaling. IL-10 and IL-17 were shown to indirectly regulate chemokine mRNA stability in neutrophils (47, 48); therefore, it is possible that the increased C1qb expression in *Il1a*<sup>-/-</sup> neutrophils is a consequence of IL-1 $\alpha$  regulating C1qb mRNA stability. Overall, further studies in this area will increase our understanding of host-pathogen interactions in infected corneas and may identify novel targets for therapeutic intervention.

## Supplementary Material

Refer to Web version on PubMed Central for supplementary material.

## Acknowledgments

We thank Martin Minns, Tatiane Lima, Francesco Marangoni, Melissa Lodoen, and Armando Villalta for helpful discussions. We are grateful to Karl Liboro (Pearlman laboratory, UCI), Jennifer Atwood (UCI flow cytometry core), Christina Lin (UCI Genomics core), Yi-Liu Xie (Histology), Angel Ayala and Matt Inlay (UCI), Feng Lin (Cleveland Clinic Foundation), and Andrea Tenner (UCI) for technical support and providing reagents.

This work was supported by National Institutes of Health Grants RO1 EY14362 (to E.P.) and F31 EY032312-02 (to B.R.). The authors also received departmental support from an unrestricted grant to the Department of Ophthalmology from the Research to Prevent Blindness Foundation (New York, NY).

## Abbreviations:

<b>AUC</b>	area under the curve
<b>BMDC</b>	bone marrow–derived dendritic cell
<b>DKO</b>	double knockout
<b>H3Cit</b>	citrullinated histone 3
<b>hpi</b>	hours postinfection
<b>KO</b>	knockout
<b>MFI</b>	mean fluorescent intensity
<b>MOI</b>	multiplicity of infection
<b>NETosis</b>	neutrophil extracellular trap formation
<b>ROS</b>	reactive oxygen species
<b>RNA-seq</b>	RNA sequencing
<b>T3SS</b>	type III secretion system
<b>UCI</b>	University of California Irvine
<b>WT</b>	wild-type

## References

1. Ung L, Bispo PJM, Shanbhag SS, Gilmore MS, and Chodosh J. 2019. The persistent dilemma of microbial keratitis: global burden, diagnosis, and antimicrobial resistance. *Surv. Ophthalmol* 64: 255–271. [PubMed: 30590103]
2. Ratitong B, and Pearlman E. 2021. Pathogenic *Aspergillus* and *Fusarium* as important causes of blinding corneal infections—the role of neutrophils in fungal killing, tissue damage and cytokine production. *Curr. Opin. Microbiol* 63: 195–203. [PubMed: 34419783]
3. Al-Mujaini A, Al-Kharusi N, Thakral A, and Wali UK. 2009. Bacterial keratitis: perspective on epidemiology, clinico-pathogenesis, diagnosis and treatment. *Sultan Qaboos Univ. Med. J* 9: 184–195. [PubMed: 21509299]
4. Karthikeyan RS, Priya JL, Leal SM Jr., Toska J, Rietsch A, Prajna V, Pearlman E, and Lalitha P. 2013. Host response and bacterial virulence factor expression in *Pseudomonas aeruginosa* and *Streptococcus pneumoniae* corneal ulcers. *PLoS One* 8: e64867. [PubMed: 23750216]
5. Karmakar M, Sun Y, Hise AG, Rietsch A, and Pearlman E. 2012. Cutting edge: IL-1 $\beta$  processing during *Pseudomonas aeruginosa* infection is mediated by neutrophil serine proteases and is independent of NLRC4 and caspase-1. *J. Immunol* 189: 4231–4235. [PubMed: 23024281]
6. Rudner XL, Kernacki KA, Barrett RP, and Hazlett LD. 2000. Prolonged elevation of IL-1 in *Pseudomonas aeruginosa* ocular infection regulates macrophage-inflammatory protein-2 production, polymorphonuclear neutrophil persistence, and corneal perforation. *J. Immunol* 164: 6576–6582. [PubMed: 10843717]
7. Karthikeyan RS, Leal SM Jr., Prajna NV, Dharmalingam K, Geiser DM, Pearlman E, and Lalitha P. 2011. Expression of innate and adaptive immune mediators in human corneal tissue infected with *Aspergillus* or *fusarium*. *J. Infect. Dis* 204: 942–950. [PubMed: 21828275]

8. Sun Y, Karmakar M, Roy S, Ramadan RT, Williams SR, Howell S, Shive CL, Han Y, Stopford CM, Rietsch A, and Pearlman E. 2010. TLR4 and TLR5 on corneal macrophages regulate *Pseudomonas aeruginosa* keratitis by signaling through MyD88-dependent and -independent pathways. *J. Immunol* 185: 4272–4283. [PubMed: 20826748]
9. Di Paolo NC, and Shayakhmetov DM. 2016. Interleukin 1 $\alpha$  and the inflammatory process. *Nat. Immunol* 17: 906–913. [PubMed: 27434011]
10. Scarpa M, Kessler S, Sadler T, West G, Homer C, McDonald C, de la Motte C, Fiocchi C, and Stylianou E. 2015. The epithelial danger signal IL-1 $\alpha$  is a potent activator of fibroblasts and reactivator of intestinal inflammation. *Am. J. Pathol* 185: 1624–1637. [PubMed: 25864926]
11. Fukuda K, Ishida W, Miura Y, Kishimoto T, and Fukushima A. 2017. Cytokine expression and barrier disruption in human corneal epithelial cells induced by alarmin released from necrotic cells. *Jpn. J. Ophthalmol* 61: 415–422. [PubMed: 28725984]
12. Ratitong B, Marshall M, and Pearlman E. 2021.  $\beta$ -Glucan-stimulated neutrophil secretion of IL-1 $\alpha$  is independent of GSDMD and mediated through extracellular vesicles. *Cell Rep.* 35: 109139. [PubMed: 34010648]
13. Franchi L, Eigenbrod T, Muñoz-Planillo R, and Nuñez G. 2009. The inflammasome: a caspase-1-activation platform that regulates immune responses and disease pathogenesis. *Nat. Immunol* 10: 241–247. [PubMed: 19221555]
14. Gross O, Yazdi AS, Thomas CJ, Masin M, Heinz LX, Guarda G, Quadroni M, Drexler SK, and Tschopp J. 2012. Inflammasome activators induce interleukin-1 $\alpha$  secretion via distinct pathways with differential requirement for the protease function of caspase-1. *Immunity* 36: 388–400. [PubMed: 22444631]
15. Wessendorf JH, Garfinkel S, Zhan X, Brown S, and Maciag T. 1993. Identification of a nuclear localization sequence within the structure of the human interleukin-1 alpha precursor. *J. Biol. Chem* 268: 22100–22104. [PubMed: 8408068]
16. Malik A, and Kanneganti T-D. 2018. Function and regulation of IL-1 $\alpha$  in inflammatory diseases and cancer. *Immunol. Rev* 281: 124–137. [PubMed: 29247991]
17. Horai R, Asano M, Sudo K, Kanuka H, Suzuki M, Nishihara M, Takahashi M, and Iwakura Y. 1998. Production of mice deficient in genes for interleukin (IL)-1 $\alpha$ , IL-1 $\beta$ , IL-1 $\alpha/\beta$ , and IL-1 receptor antagonist shows that IL-1 $\beta$  is crucial in turpentine-induced fever development and glucocorticoid secretion. *J. Exp. Med* 187: 1463–1475. [PubMed: 9565638]
18. Pearlman E, Sun Y, Roy S, Karmakar M, Hise AG, Szczotka-Flynn L, Ghannoum M, Chinnery HR, McMenamin PG, and Rietsch A. 2013. Host defense at the ocular surface. *Int. Rev. Immunol* 32: 4–18. [PubMed: 23360155]
19. Thanabalasuriar A, Scott BNV, Peiseler M, Willson ME, Zeng Z, Warren P, Keller AE, Surewaard BGJ, Dozier EA, Korhonen JT, et al. 2019. Neutrophil extracellular traps confine *Pseudomonas aeruginosa* ocular biofilms and restrict brain invasion. *Cell Host Microbe* 25: 526–536.e4. [PubMed: 30930127]
20. Vareechon C, Zmina SE, Karmakar M, Pearlman E, and Rietsch A. 2017. *Pseudomonas aeruginosa* effector ExoS inhibits ROS production in human neutrophils. *Cell Host Microbe* 21: 611–618.e5. [PubMed: 28494242]
21. Rivers-Auty J, Daniels MJD, Colliver I, Robertson DL, and Brough D. 2018. Redefining the ancestral origins of the interleukin-1 superfamily. *Nat. Commun* 9: 1156. [PubMed: 29559685]
22. Rider P, Carmi Y, Voronov E, and Apte RN. 2013. Interleukin-1 $\alpha$ . *Semin. Immunol* 25: 430–438. [PubMed: 24183701]
23. Luheshi NM, Rothwell NJ, and Brough D. 2009. The dynamics and mechanisms of interleukin-1 $\alpha$  and  $\beta$  nuclear import. *Traffic* 10: 16–25. [PubMed: 18939951]
24. Zhou Y, Zhou B, Pache L, Chang M, Khodabakhshi AH, Tanaseichuk O, Benner C, and Chanda SK. 2019. Metascape provides a biologist-oriented resource for the analysis of systems-level datasets. *Nat. Commun* 10: 1523. [PubMed: 30944313]
25. Thielens NM, Tedesco F, Bohlson SS, Gaboriaud C, and Tenner AJ. 2017. C1q: a fresh look upon an old molecule. *Mol. Immunol* 89: 73–83. [PubMed: 28601358]

26. Thakur A, Barrett RP, McClellan S, and Hazlett LD. 2004. Regulation of *Pseudomonas aeruginosa* corneal infection in IL-1 beta converting enzyme (ICE, caspase-1) deficient mice. *Curr. Eye Res* 29: 225–233. [PubMed: 15590467]
27. Sun Y, Abbondante S, Karmakar M, de Jesus Carrion S, Che C, Hise AG, and Pearlman E. 2018. Neutrophil caspase-11 is required for cleavage of caspase-1 and secretion of IL-1 $\beta$  in *Aspergillus fumigatus* infection. *J. Immunol* 201: 2767–2775. [PubMed: 30266768]
28. Hauser AR. 2009. The type III secretion system of *Pseudomonas aeruginosa*: infection by injection. *Nat. Rev. Microbiol* 7: 654–665. [PubMed: 19680249]
29. Frithz-Lindsten E, Du Y, Rosqvist R, and Forsberg A. 1997. Intracellular targeting of exoenzyme S of *Pseudomonas aeruginosa* via type III-dependent translocation induces phagocytosis resistance, cytotoxicity and disruption of actin microfilaments. *Mol. Microbiol* 25: 1125–1139. [PubMed: 9350868]
30. Finck-Barbançon V, Goranson J, Zhu L, Sawa T, Wiener-Kronish JP, Fleiszig SM, Wu C, Mende-Mueller L, and Frank DW. 1997. ExoU expression by *Pseudomonas aeruginosa* correlates with acute cytotoxicity and epithelial injury. *Mol. Microbiol* 25: 547–557. [PubMed: 9302017]
31. Al Moussawi K, and Kazmierczak BI. 2014. Distinct contributions of interleukin-1 $\alpha$  (IL-1 $\alpha$ ) and IL-1 $\beta$  to innate immune recognition of *Pseudomonas aeruginosa* in the lung. *Infect. Immun* 82: 4204–4211. [PubMed: 25069982]
32. Barry KC, Fontana MF, Portman JL, Dugan AS, and Vance RE. 2013. IL-1 $\alpha$  signaling initiates the inflammatory response to virulent *Legionella pneumophila* in vivo. *J. Immunol* 190: 6329–6339. [PubMed: 23686480]
33. Eislmayr K, Bestehorn A, Morelli L, Borroni M, Walle LV, Lamkanfi M, and Kovarik P. 2022. Nonredundancy of IL-1 $\alpha$  and IL-1 $\beta$  is defined by distinct regulation of tissues orchestrating resistance versus tolerance to infection. *Sci. Adv* 8: eabj7293. [PubMed: 35235356]
34. Caffrey-Carr AK, Kowalski CH, Beattie SR, Blaseg NA, Upshaw CR, Thammahong A, Lust HE, Tang Y-W, Hohl TM, Cramer RA, and Obar JJ. 2017. Interleukin 1 $\alpha$  is critical for resistance against highly virulent *Aspergillus fumigatus* isolates. *Infect. Immun* 85: e00661–17. [PubMed: 28947643]
35. Caffrey AK, Lehmann MM, Zickovich JM, Espinosa V, Shepardson KM, Watschke CP, Hilmer KM, Thammahong A, Barker BM, Rivera A, et al. 2015. IL-1 $\alpha$  signaling is critical for leukocyte recruitment after pulmonary *Aspergillus fumigatus* challenge. *PLoS Pathog.* 11: e1004625. [PubMed: 25629406]
36. Fields JK, Günther S, and Sundberg EJ. 2019. Structural basis of IL-1 family cytokine signaling. *Front. Immunol* 10: 1412. [PubMed: 31281320]
37. Lin X, Twelkmeyer T, Wang S-Y, Xu R-N, Wang F-S, Zhang C, and Tang H. 2020. An immunopathogenic perspective of interleukin-1 signaling. *Cell. Mol. Immunol* 17: 892–893. [PubMed: 32467618]
38. Bersudsky M, Luski L, Fishman D, White RM, Ziv-Sokolovskaya N, Dotan S, Rider P, Kaplanov I, Aychek T, Dinarello CA, et al. 2014. Non-redundant properties of IL-1 $\alpha$  and IL-1 $\beta$  during acute colon inflammation in mice. *Gut* 63: 598–609. [PubMed: 23793223]
39. Voronov E, Dotan S, Krelin Y, Song X, Elkabets M, Carmi Y, Rider P, Cohen I, Romzova M, Kaplanov I, and Apte RN. 2013. Unique versus redundant functions of IL-1 $\alpha$  and IL-1 $\beta$  in the tumor microenvironment. *Front. Immunol* 4: 177. [PubMed: 23847618]
40. Nazarenko I, Marhaba R, Reich E, Voronov E, Vitacolonna M, Hildebrand D, Elter E, Rajasagi M, Apte RN, and Zöller M. 2008. Tumorigenicity of IL-1 $\alpha$ - and IL-1 $\beta$ -deficient fibrosarcoma cells. *Neoplasia* 10: 549–562. [PubMed: 18516292]
41. Benjamin JT, Moore DJ, Bennett C, van der Meer R, Royce A, Loveland R, and Wynn JL. 2018. Cutting edge: IL-1 $\alpha$  and not IL-1 $\beta$  drives IL-1R1-dependent neonatal murine sepsis lethality. *J. Immunol* 201: 2873–2878. [PubMed: 30305325]
42. McMahan CJ, Slack JL, Mosley B, Cosman D, Lupton SD, Brunton LL, Grubin CE, Wignall JM, Jenkins NA, Brannan CI, et al. 1991. A novel IL-1 receptor, cloned from B cells by mammalian expression, is expressed in many cell types. *EMBO J.* 10: 2821–2832. [PubMed: 1833184]
43. Peters VA, Joesting JJ, and Freund GG. 2013. IL-1 receptor 2 (IL-1R2) and its role in immune regulation. *Brain Behav. Immun* 32: 1–8. [PubMed: 23195532]

44. Bora NS, Jha P, and Bora PS. 2008. The role of complement in ocular pathology. *Semin. Immunopathol* 30: 85–95. [PubMed: 18299835]
45. Ricklin D, Reis ES, Mastellos DC, Gros P, and Lambris JD. 2016. Complement component C3—the “Swiss Army Knife” of innate immunity and host defense. *Immunol. Rev* 274: 33–58. [PubMed: 27782325]
46. Bobak DA, Gaither TA, Frank MM, and Tenner AJ. 1987. Modulation of FcR function by complement: subcomponent C1q enhances the phagocytosis of IgG-opsonized targets by human monocytes and culture-derived macrophages. *J. Immunol* 138: 1150–1156. [PubMed: 3492544]
47. Biswas R, Datta S, Gupta JD, Novotny M, Tebo J, and Hamilton TA. 2003. Regulation of chemokine mRNA stability by lipopolysaccharide and IL-10. *J. Immunol* 170: 6202–6208. [PubMed: 12794151]
48. Hamilton T, Li X, Novotny M, Pavicic PG Jr., Datta S, Zhao C, Hartupee J, and Sun D. 2012. Cell type- and stimulus-specific mechanisms for post-transcriptional control of neutrophil chemokine gene expression. *J. Leukoc. Biol* 91: 377–383. [PubMed: 22167720]

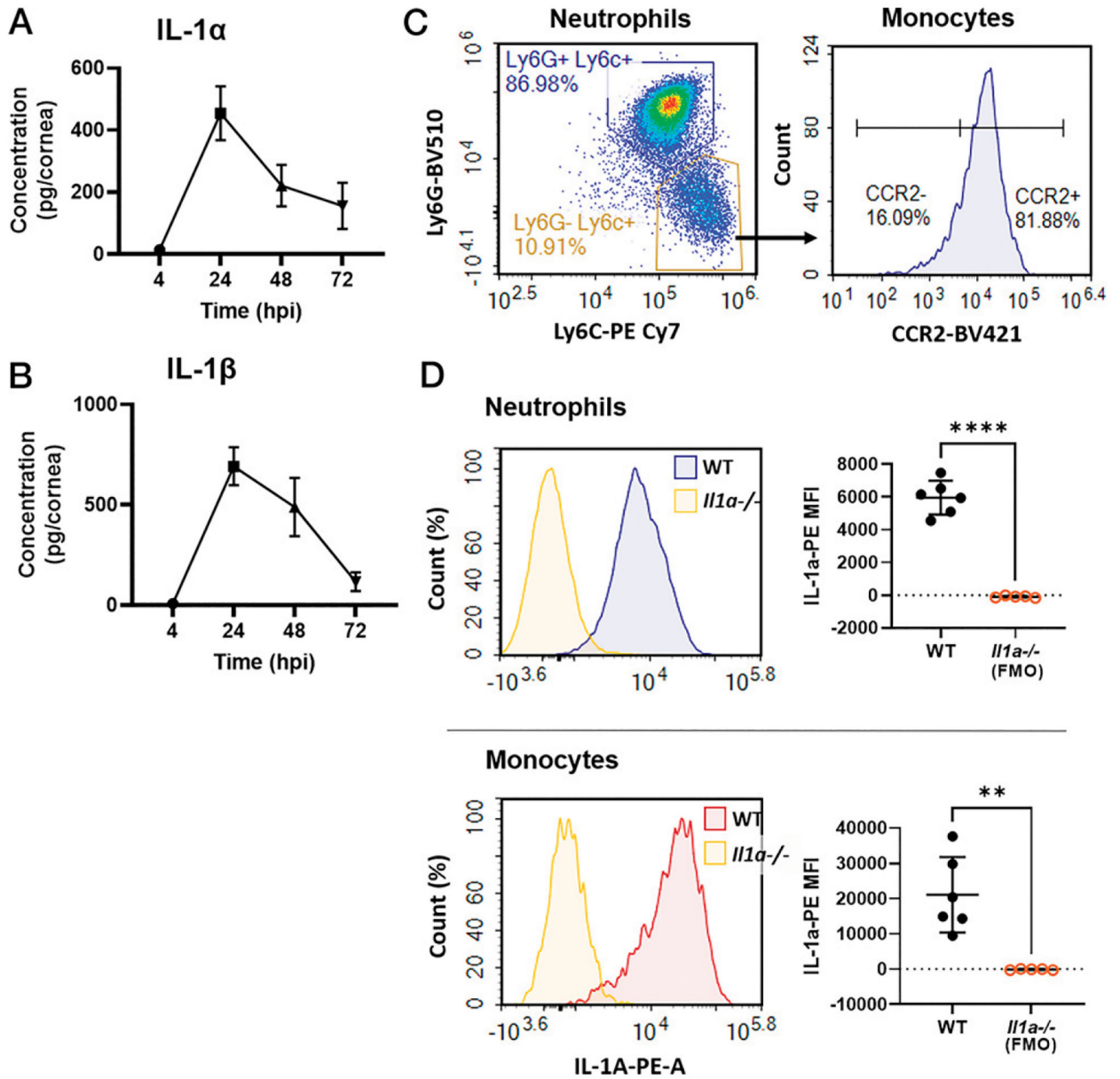


**FIGURE 1. IL-1 $\alpha$  production in *P. aeruginosa* keratitis.**

(A and B) Time course of IL-1 $\alpha$  and IL-1 $\beta$  production in *P. aeruginosa* (PAO1)-infected corneas of C57BL/6 (WT) mice quantified by ELISA ( $n = 8$  biological replicates, repeated twice). (C) Flow cytometry of live, single CD45<sup>+</sup>CD11b<sup>+</sup> cells at 24 hpi showing neutrophils (Ly6G<sup>+</sup>Ly6C<sup>+</sup>) and monocytes (Ly6G<sup>-</sup>Ly6C<sup>hi</sup>CCR2<sup>+</sup>). (D) Intracellular IL-1 $\alpha$ <sup>+</sup> (PE) neutrophils and monocytes shown as representative histograms (left). MFI was quantified using *Il1a*<sup>-/-</sup> cells as the fluorescence minus one (FMO) control (right).  $n = 5$ –6 biological replicates, repeated twice. \*\* $p < 0.01$ , \*\*\*\* $p < 0.0001$ , determined by ordinary one-way ANOVA with Tukey's multiple comparisons test.

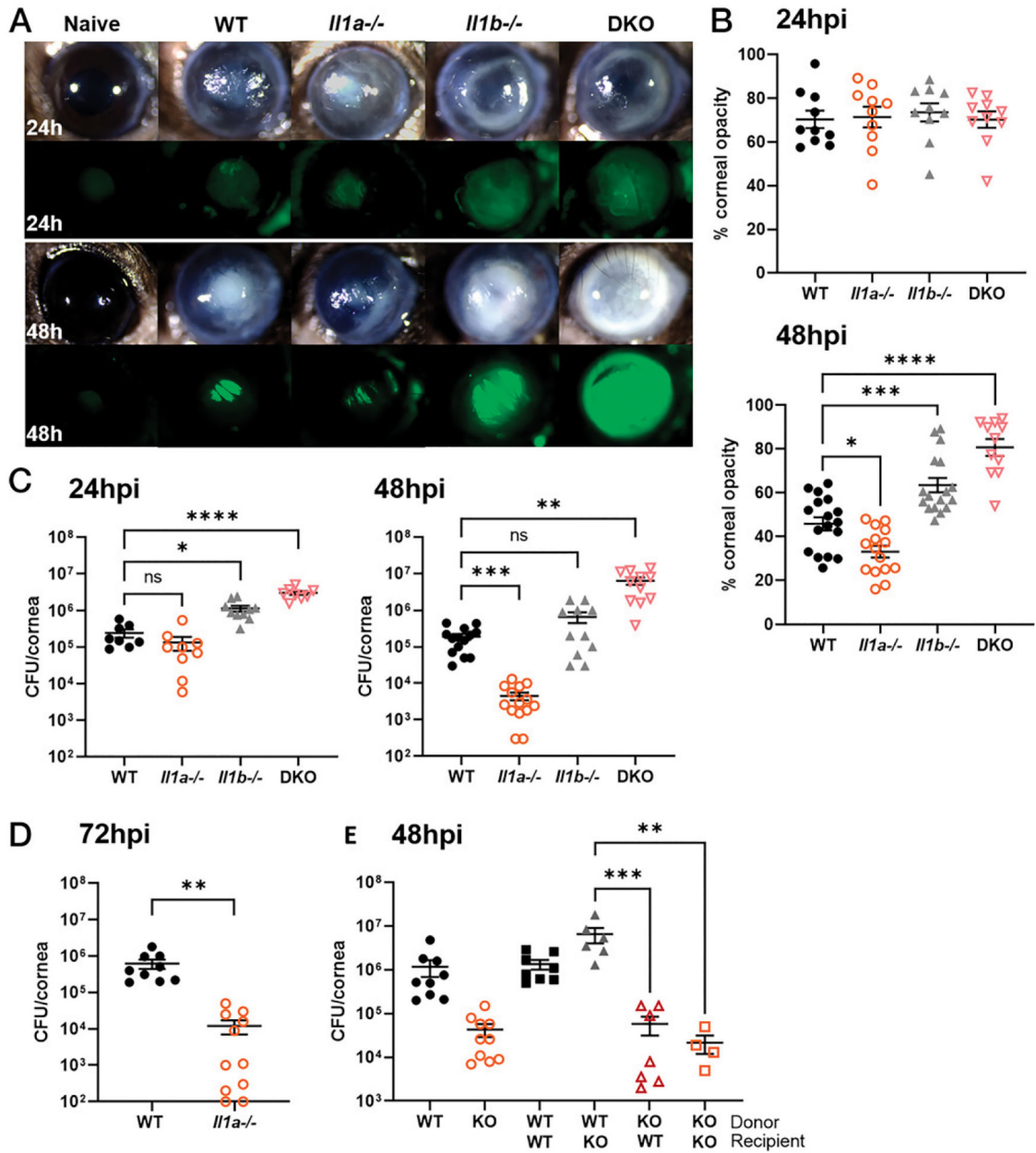


**FIGURE 2. The role of IL-1 $\alpha$  and IL-1 $\beta$  in *P. aeruginosa* keratitis.**

Corneas of WT, *Il1a*<sup>-/-</sup>, *Il1b*<sup>-/-</sup>, and DKO mice infected with  $5 \times 10^4$  PAO1 expressing GFP and examined at 24 and 48 hpi. (A) Representative images of corneal opacity (brightfield) and GFP (bacteria) in infected WT, *Il1a*<sup>-/-</sup>, *Il1b*<sup>-/-</sup>, and DKO mice. (B) Quantification of percent corneal opacity by ImageJ. (C and D) Live bacteria from infected corneas quantified by CFUs at (C) 24, 48, and (D) 72 hpi. (E) CFUs in bone marrow transplant mice at 48 hpi.  $n = 8-10$  corneas for 24 and 72 hpi time points, experiment repeated three times, and  $n = 10-20$  corneas for 48 hpi time point repeated four times.  $n = 5-10$  corneas for bone marrow transplant; experiments were repeated three times. \* $p < 0.05$ , \*\* $p < 0.01$ , \*\*\* $p < 0.001$ , \*\*\*\* $p < 0.0001$ , ordinary one-way ANOVA with Dunnett's multiple comparison test

was used for (B) and (E) and left panel of (C), Brown Forsythe and Welch ANOVA test with Dunnett's T3 multiple comparison test of right panel of (C), and unpaired *t* test (D).

Author Manuscript

Author Manuscript

Author Manuscript

Author Manuscript

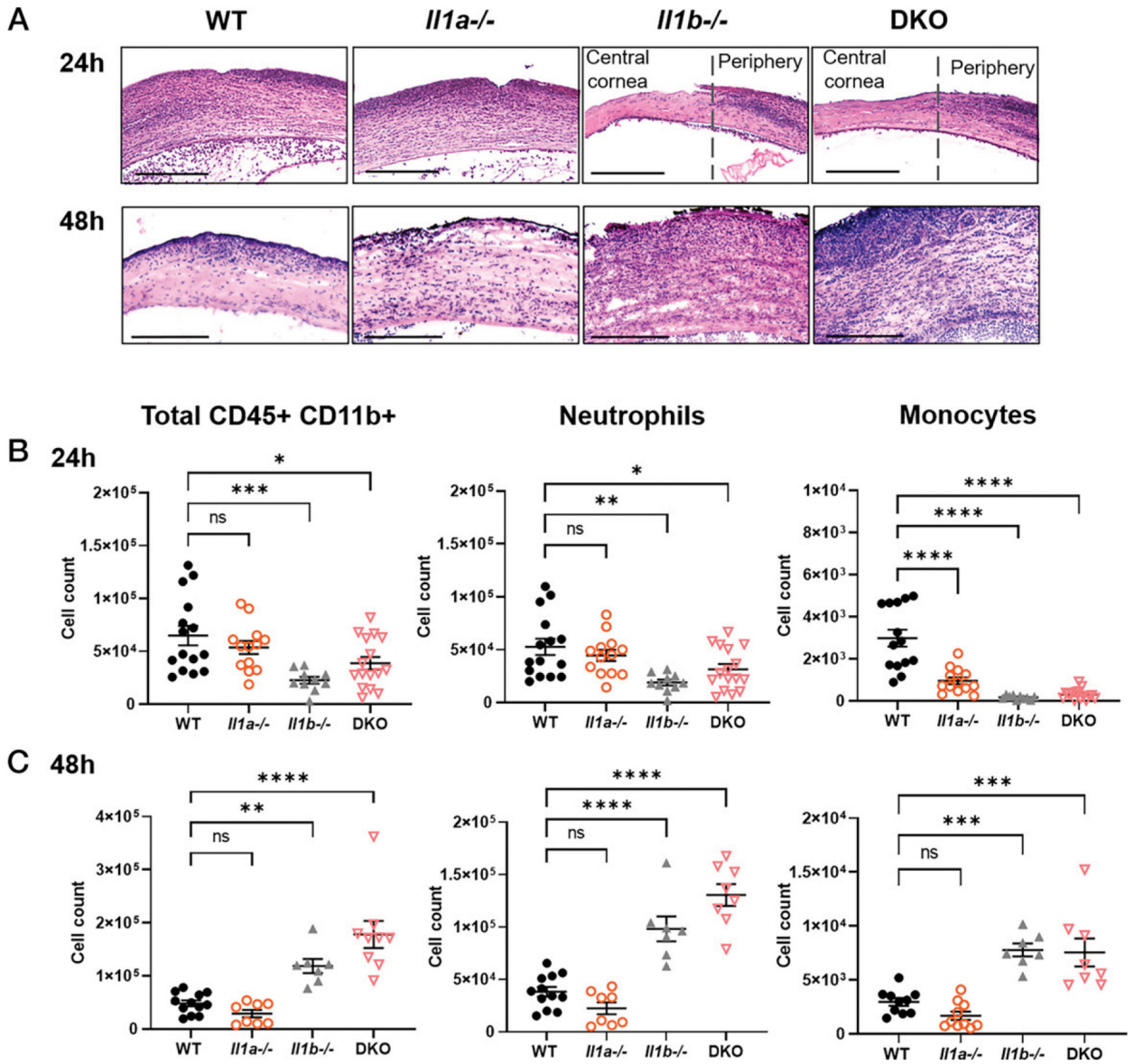


**FIGURE 3. Neutrophil and monocyte recruitment to *P. aeruginosa*-infected corneas.** (A) Representative images from H&E-stained corneal sections of infected WT, *Il1a*<sup>-/-</sup>, *Il1b*<sup>-/-</sup>, and DKO corneas. Scale bars, 200  $\mu$ M. Cellular recruitment was quantified by flow cytometry at (B) 24 and (C) 48 hpi; neutrophils were gated on CD45<sup>+</sup>CD11b<sup>+</sup>/Ly6G<sup>+</sup>Ly6C<sup>+</sup>, and monocytes were gated on Ly6G<sup>-</sup>Ly6C<sup>hi</sup>CCR2<sup>+</sup> (Supplemental Fig. 2B).  $n = 5$  biological replicates, three repeat experiments (A);  $n = 10$ –15, four repeat experiments (B and C). \* $p < 0.05$ , \*\* $p < 0.01$ , \*\*\* $p < 0.001$ , \*\*\*\* $p < 0.0001$ , using ordinary one-way ANOVA with Dunnett’s multiple comparisons test.

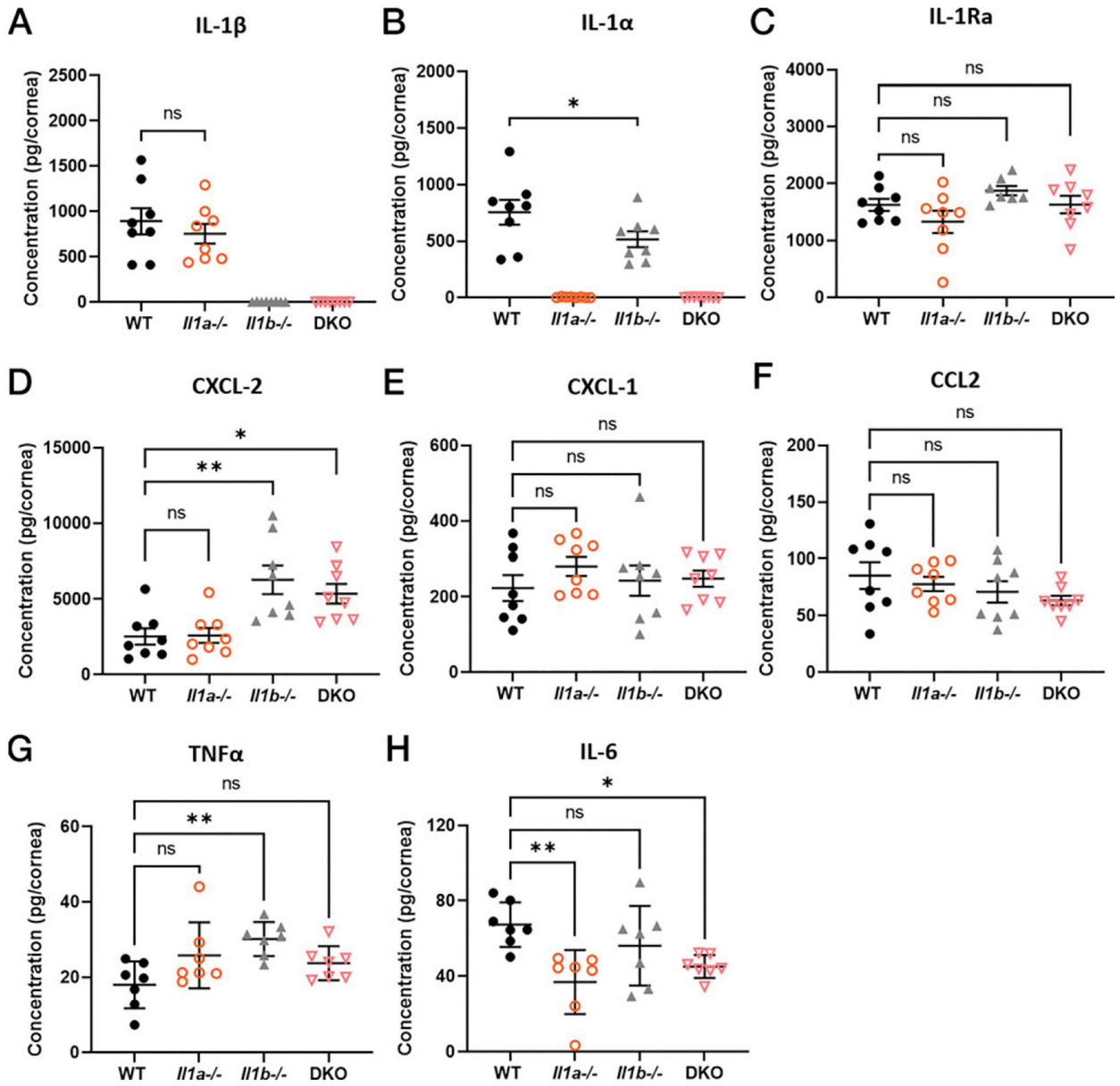


**FIGURE 4. Cytokine production in infected WT, *Il1a*<sup>-/-</sup>, and *Il1b*<sup>-/-</sup> corneas.** PAO1-infected corneas from WT, *Il1a*<sup>-/-</sup>, *Il1b*<sup>-/-</sup>, and DKO mice were homogenized at 24 hpi, and cytokines were quantified by ELISA. (A) IL-1β, (B) IL-1α, (C) IL-1Ra, (D) CXCL-2, (E) CXCL-1, (F) CCL2, (G) TNFα, and (H) IL-6 concentration was calculated as pg/cornea (three repeated experiments). \**p* < 0.05, \*\**p* < 0.01, using ordinary one-way ANOVA with Dunnett's multiple comparisons test.

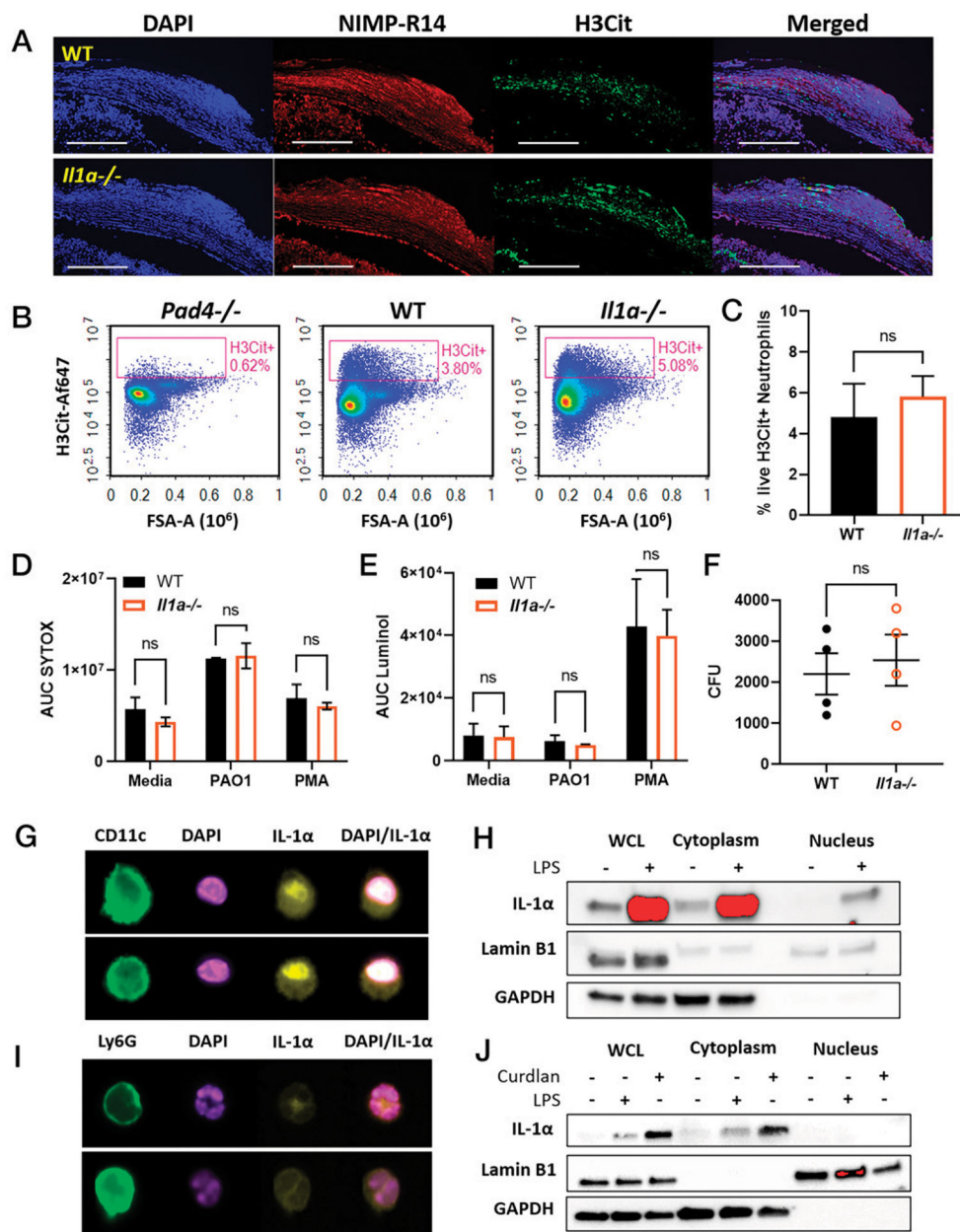


**FIGURE 5. Neutrophil effector functions and IL-1 $\alpha$  nuclear localization.**

(A) Representative images of WT and *Il1a*<sup>-/-</sup> corneal sections at 24 hpi with NIMP-R14 (neutrophils), and H3Cit as an indicator of NETosis (representative of  $n = 6$  mice, three repeat experiments). (B) Flow cytometry of intracellular H3Cit in ex vivo neutrophils from infected WT, *Pad4*<sup>-/-</sup>, and *Il1a*<sup>-/-</sup>. (C) Quantification of % H3Cit<sup>+</sup>Ly6G<sup>+</sup> neutrophils ( $n = 4$ ). (D–F) In vitro functional analysis of peritoneal neutrophils from WT and *Il1a*<sup>-/-</sup> mice stimulated with PMA or PAO1 ( $n = 3$  repeated experiments). (D) Extracellular DNA quantified by AUC. (E) Total ROS quantified as AUC of luminol fluorescence. (F) Neutrophil killing of phagocytosed PAO1 quantified by CFUs. (G and H) Nuclear localization in LPS-stimulated BMDCs. (G) Imaging flow cytometry of IL-1 $\alpha$  (yellow) and nuclei (DAPI). (H) Cytoplasmic and nuclear extracts analyzed by Western blot for IL-1 $\alpha$ ,

Lamin B1 (nuclei), and GAPDH (cytosol). (I) Localization of IL-1 $\alpha$  in  $\beta$ -glucan-stimulated neutrophils (curdlan) examined by imaging flow cytometry. (J) Neutrophil cytoplasmic and nuclear extract analyzed by Western blot for IL-1 $\alpha$ . Imaging flow cytometry and Western blot experiments were repeated three times. Western blot membrane images were cropped to show bands at the corresponding molecular weights. Ordinary one-way ANOVA with Dunnett's multiple comparisons test was used for (B) and (C); unpaired *t* test was used for (D).

Author Manuscript

Author Manuscript

Author Manuscript

Author Manuscript

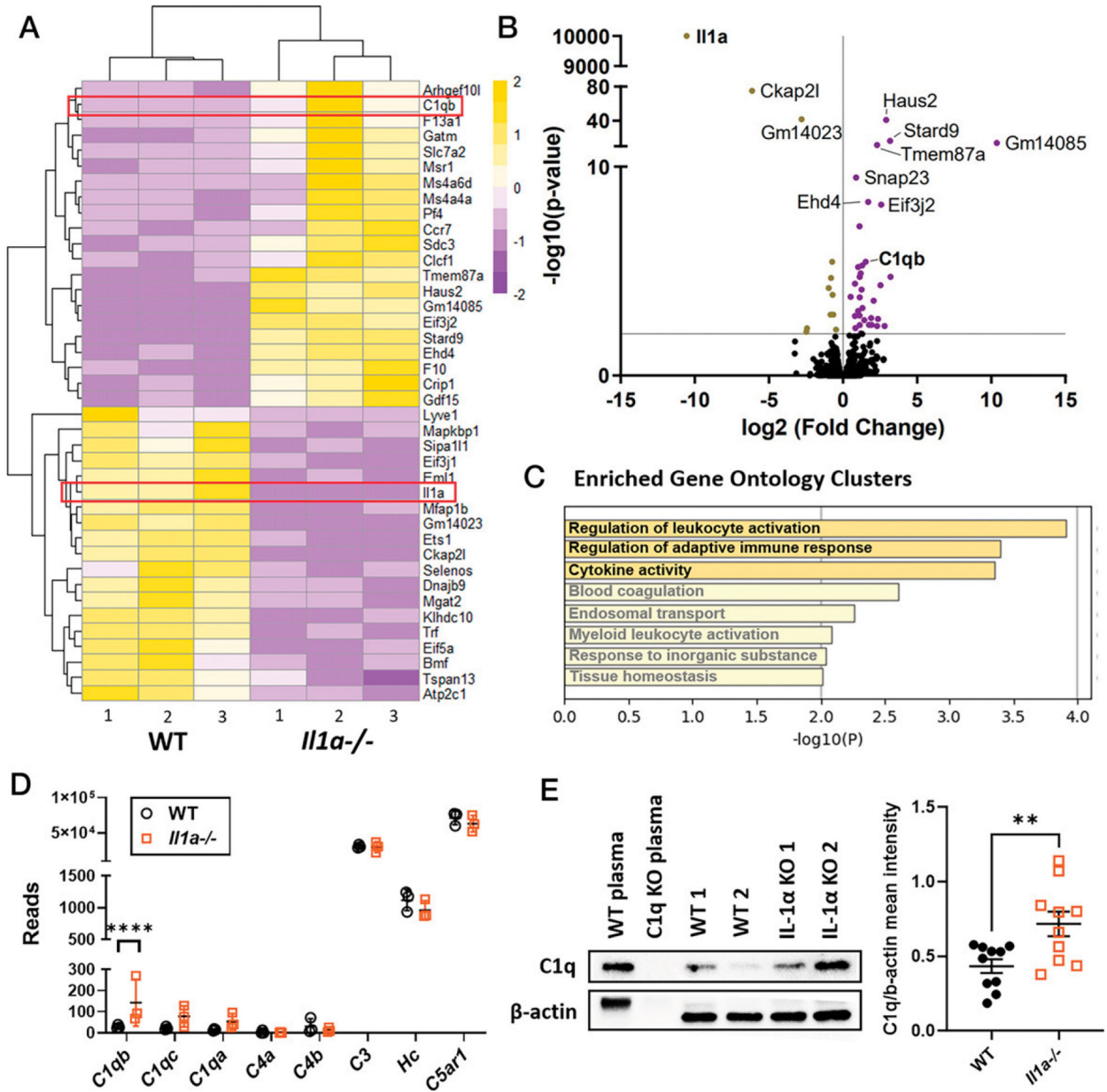


**FIGURE 6. Transcriptomic analysis of WT and *Il1a*<sup>-/-</sup> neutrophils from infected corneas.** Bulk RNA-seq of live Ly6G<sup>+</sup>Ly6C<sup>+</sup>CD45<sup>+</sup>CD11b<sup>+</sup> neutrophils sorted from infected WT and *Il1a*<sup>-/-</sup> corneas at 24 hpi (*n* = 3). **(A)** Heatmap showing the top 30 differentially expressed genes, with yellow indicative of upregulation and purple showing downregulated genes. **(B)** Volcano plot of DE genes. Genes were filtered for subsequent analysis using the following cutoff: fold change > 2; adjusted *p* < 0.05. **(C)** Gene Ontology (GO) terms associated with genes that are upregulated in *Il1a*<sup>-/-</sup> corneal neutrophils (<https://metascape.org>). **(D)** Complement gene reads expressed by neutrophils from infected WT and *Il1a*<sup>-/-</sup> corneas. **(E)** Representative Western blot of C1q in infected corneas from WT and *Il1a*<sup>-/-</sup> mice (left), and quantification of band intensity normalized to β-actin loading control (right). *n* = 3 samples,

each containing neutrophils from four pooled corneas. For (E),  $n = 10$  biological replicates from three independent experiments.  $**p < 0.01$ ,  $****p < 0.0001$ , unpaired  $t$  test.

Author Manuscript

Author Manuscript

Author Manuscript

Author Manuscript